International Journal of Engineering Research & Technology (IJERT)
ISSN: 2278-0181
Vol. 15 Issue 06 , June - 2026

Active Cell Balancing of Series-Connected Lithium-Ion Battery Cells using an Isolated Flyback Converter

Poonam Shetti[1], Sanjay N. Patil[2]
[1] Research Scholar, Department of Electrical Engineering, PVPIT, Budhagaon, Sangli, Maharashtra, India
[2] Associate Professor, Department of Electrical Engineering, PVPIT, Budhagaon, Sangli, Maharashtra, India

Abstract—Lithium-ion battery packs used in electric vehicles (EVs) and grid energy-storage systems comprise large numbers of series-connected cells that gradually develop voltage and state-of-charge (SOC) mismatches because of manufacturing tolerances, temperature gradients and uneven aging. Such imbalance reduces usable capacity, accelerates degradation and threatens pack safety, making cell balancing an indispensable function of any modern battery management system (BMS). This paper presents the design, simulation and hardware realization of an active cell-balancing scheme based on an isolated flyback converter that transfers energy from a higher-SOC cell to a lower-SOC cell instead of dissipating it as heat. The flyback topology is selected for its galvanic isolation, low component count and flexible cell-to-pack energy routing. A SOC-based balancing algorithm regulates the converter duty cycle and gate pulses. A MATLAB/Simulink model of a two-cell system is developed for both passive (resistive) and active (flyback) balancing, and a 3.7 V hardware prototype controlled by an Arduino Uno is built to validate the simulation. Results show that active balancing equalizes a 5% SOC mismatch in 235 s in simulation (47 s per percent), against 484 s for passive balancing. The hardware prototype balances a 10% mismatch in 760 s with the flyback converter (76 s per percent) compared with 950 s for resistive balancing (95 s per percent), confirming the superior speed and efficiency of the proposed active method.

Index Terms—Active cell balancing, flyback converter, lithium-ion battery, state of charge, battery management system, electric vehicle.

I. INTRODUCTION

The rapid electrification of transportation and the expansion of grid-scale renewable energy storage have made the lithium-ion battery the dominant electrochemical energy-storage technology, owing to its high energy density, low self-discharge and absence of memory effect [1]. To meet the voltage and capacity demands of these applications, hundreds or even thousands of individual cells are connected in series and parallel. Ideally every cell in a string would behave identically; in practice, however, packs are highly susceptible to string unbalance caused by manufacturing variances in internal resistance and capacity, together with operational factors such as thermal gradients and uneven aging rates [2], [3].

Cell imbalance is not a minor inconvenience. When series-connected cells diverge in SOC, the weakest cell limits both the charge and discharge of the entire pack: charging must stop when the highest cell reaches its upper voltage limit, while discharging must stop when the lowest cell reaches its cut-off, leaving usable energy stranded in the remaining cells. Persistent imbalance also accelerates capacity fade and, in extreme cases, can drive a cell into overcharge or deep discharge with attendant risks of thermal runaway [4]. Cell balancing has therefore become an indispensable regulatory function integrated into modern battery management systems (BMS) to mitigate accelerated aging, recover lost pack capacity and prevent catastrophic safety hazards [5], [6].

Balancing techniques are broadly classified as passive or active [6], [9]. Passive balancing dissipates the excess energy of higher-voltage cells as heat through shunt resistors until all cells reach the level of the weakest cell. It is simple, inexpensive and compact, which keeps it the dominant choice for consumer electronics and low-power systems [9], [11]. However, it wastes energy, generates localized heat and balances only at the lowest cell SOC, making it increasingly unattractive as pack size and energy demand grow. Active balancing instead redistributes charge from high-energy cells to low-energy cells using non-dissipative storage elements such as capacitors, inductors, transformers or DC–DC converters [10], [12], [13]. This conserves energy, reduces thermal stress, increases balancing speed and improves usable capacity, which is decisive for high-energy EV and stationary-storage applications.

International Journal of Engineering Research & Technology (IJERT)
ISSN: 2278-0181
Vol. 15 Issue 06 , June - 2026

Among the converter-based active methods, the isolated flyback converter is particularly attractive. Through its multi-winding high-frequency transformer it provides galvanic isolation between cells, allows flexible cell-to-cell or cell-to-pack energy routing, and bypasses the adjacent-cell bottleneck that limits non-isolated buck–boost and switched-capacitor schemes [14]–[18]. These advantages have motivated several flyback-based balancing designs for EV and renewable-storage packs [16], [17], [20].

The objective of the present work is to design, simulate and experimentally implement a flyback-converter-based charge balancer for series-connected lithium-ion cells used in EV applications. Specifically, the work develops a SOC-based balancing algorithm, models both passive and active balancing in MATLAB/Simulink, builds an Arduino-controlled hardware prototype, and quantitatively compares the balancing speed of the two methods. The remainder of this paper is organized as follows. Section II describes the flyback converter, its control and the balancing algorithm. Section III presents the MATLAB/Simulink model and simulation results for passive and active balancing. Section IV details the hardware implementation and experimental results. Section V concludes the paper and outlines the future scope.

II. FLYBACK CONVERTER AND CELL-BALANCING CONTROL

A. Principle of the Flyback Converter

The flyback converter is an isolated DC–DC converter widely used in switched-mode power supplies, battery chargers and active cell-balancing circuits. As shown in Fig. 1, it consists of an input source V_{IN}, an input capacitor C_{IN}, a transformer with primary and secondary windings L_P and L_S, a controlled MOSFET switch, a rectifier diode D, an output capacitor C_O and the load R_L. It stores energy in the transformer magnetizing inductance during the switch ON state and delivers that energy to the load during the OFF state, while a pulse-width-modulation (PWM) signal regulates the output voltage.

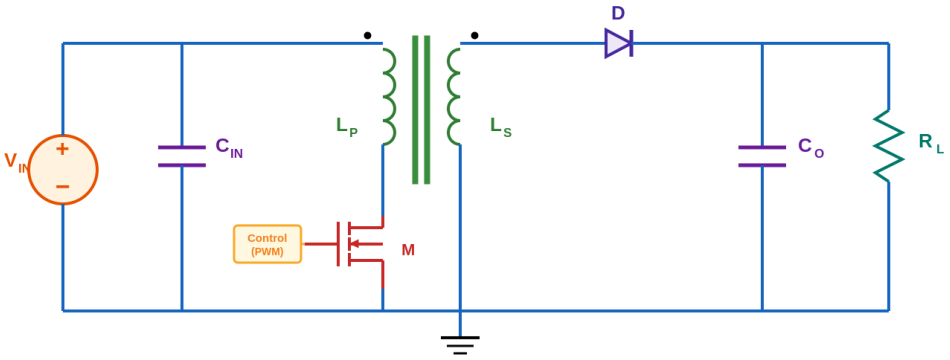

Fig. 1. Topology of the isolated flyback converter.

When the MOSFET turns ON, the input voltage is impressed across the primary winding and the primary current rises linearly while energy is stored in the core. The secondary voltage polarity reverse-biases the diode, so the load is supplied momentarily by C_O. The primary current during the ON interval is

$$i_p(t) = \frac{V_{in}}{L_p} \cdot t \tag{1}$$

and the energy stored in the magnetizing inductance is

$$E = \frac{1}{2} L_p I_p^2 \tag{2}$$

When the switch turns OFF, the magnetic field collapses, the winding polarity reverses and the diode becomes forward-biased, transferring the stored energy through the secondary to the output capacitor and load. For continuous conduction mode (CCM) the ideal output voltage is

$$V_o = \frac{N_s}{N_p} \cdot \frac{D}{1-D} \cdot V_{in} \tag{3}$$

where N_P and N_S are the primary and secondary turns and D is the duty cycle. By varying the duty cycle and turns ratio, the flyback converter can step the input voltage up or down while maintaining isolation, which makes it well suited to routing balancing energy between cells [15], [18].

B. Duty-Cycle Control of the Balancing Energy

International Journal of Engineering Research & Technology (IJERT)
ISSN: 2278-0181
Vol. 15 Issue 06 , June - 2026

In a flyback-based balancing system the duty cycle governs the amount of energy transferred from a higher-voltage cell to a lower-voltage cell in each switching period, and therefore the balancing current and balancing speed. The duty cycle and switching frequency are defined as

$$D = \frac{T_{on}}{T_s}, \quad f_s = \frac{1}{T_s} \tag{4}$$

Rearranging the CCM relation (3) gives the duty cycle required to transfer energy between cells of known voltage,

$$D = \frac{V_o N_p}{V_{in} N_s + V_o N_p} \tag{5}$$

The peak magnetizing current and the energy transferred per switching cycle are

$$I_{p,peak} = \frac{V_{cell} \cdot D \cdot T_s}{L_m} \tag{6}$$

$$E = \frac{V_{cell}^2 \cdot D^2 \cdot T_s^2}{2 L_m} \tag{7}$$

Equation (7) shows that the transferred energy grows with the square of the duty cycle, so even a small increase in D markedly raises the balancing rate. In practice the controller adjusts the duty cycle from voltage or SOC feedback using a simple proportional law,

$$D = K \cdot (V_{max} - V_{min}) \tag{8}$$

where K is the proportional gain and V_{max} and V_{min} are the potentials of the highest- and lowest-SOC cells. The duty cycle thus rises automatically when imbalance is large and falls as the cells converge. To ensure proper transformer demagnetization and to limit switching loss, transformer-saturation risk and current ripple, the duty cycle is kept below 0.5 [15], [19].

C. SOC-Based Balancing Algorithm

A SOC-based algorithm decides the direction of energy transfer for the two-cell system. The controller measures both cell voltages, estimates the SOC, evaluates the SOC difference ΔSOC and compares it with a threshold ΔSOC_TH. The balancing procedure is summarized in the following steps:

- Measure the voltages of Cell-1 and Cell-2 and estimate their SOC.
- Compute the SOC difference ΔSOC and compare it with the threshold ΔSOC_TH.
- Identify the higher-SOC cell as the source cell.
- Generate PWM pulses for the corresponding MOSFET so that energy is stored in the flyback transformer during the ON period.
- Transfer the stored energy to the lower-SOC cell during the OFF period.
- Repeat until ΔSOC falls below the threshold (≈ 0.01), then stop balancing.

This closed-loop logic continuously routes charge from the stronger to the weaker cell, ensuring fast convergence without the energy waste inherent in resistive dissipation [12], [13]. The complete decision flow is shown in Fig. 2.

The flowchart in Fig. 2 captures the operation of the SOC-based balancing routine. After starting, the controller measures the terminal voltages of Cell-1 and Cell-2 and estimates their states of charge, from which it computes the absolute SOC difference $\Delta SOC = |SOC_1 - SOC_2|$. The first decision block tests whether ΔSOC exceeds the threshold ΔSOC_TH. If it does not, the cells are already balanced and the routine branches directly to STOP. If it does, a second decision block compares SOC_1 with SOC_2 to identify the source cell. When SOC_1 is larger, PWM pulses are applied to MOSFET M1 while M2 is kept OFF, so that energy from Cell-1 is stored in the transformer; when SOC_2 is larger, the controller instead pulses M2 with M1 OFF, drawing energy from Cell-2. During the subsequent switch-OFF interval the stored magnetic energy is delivered through the secondary winding and rectifier diode to the lower-SOC cell. Control then loops back to the ΔSOC comparison, and the measure–compare–transfer cycle repeats until ΔSOC falls below the threshold, at which point balancing stops. The structure therefore guarantees that energy always flows from the higher-SOC cell to the lower-SOC cell and that switching ceases automatically once equalization is achieved, avoiding over-balancing and unnecessary switching loss.

International Journal of Engineering Research & Technology (IJERT)
ISSN: 2278-0181
Vol. 15 Issue 06 , June - 2026

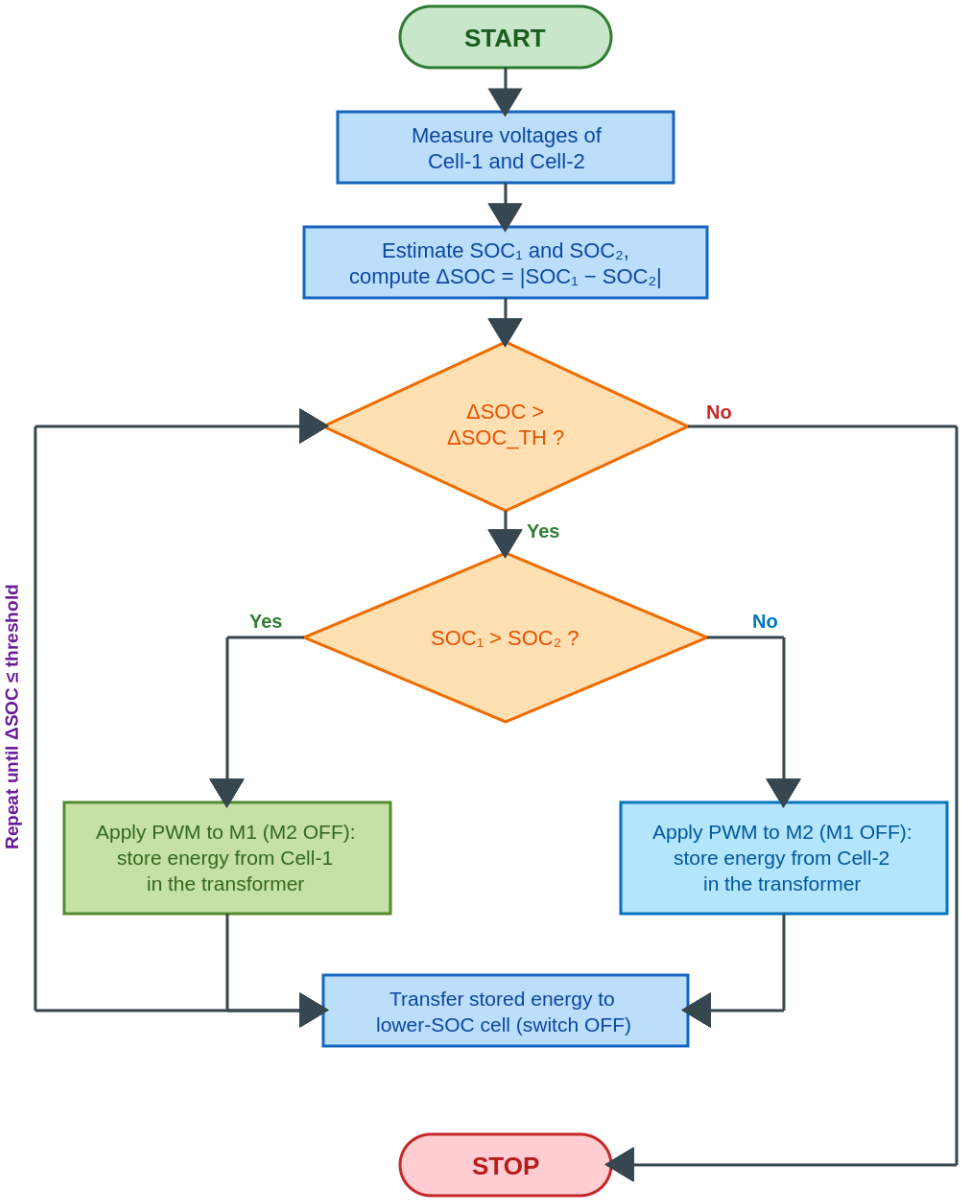

Fig. 2. Flowchart of the SOC-based active cell-balancing algorithm.

III. MATLAB/SIMULINK MODELLING AND SIMULATION RESULTS

A. Simulation Model

A hybrid two-cell battery-balancing system incorporating both passive (resistive) and active (flyback) balancing was modelled in MATLAB/Simulink, as shown in Fig. 3. The model is implemented in a discrete environment with a sampling time of 5×10^{-5} s using the powergui block. Two series-connected lithium-ion cells are monitored through SOC-measurement blocks. In the passive section, switches connect balancing resistors across each cell so that an over-charged cell discharges through its resistor as heat. In the active section, MOSFETs M1 and M2, the flyback transformer, rectifier diodes and output filters transfer energy from the higher-energy cell to the lower-energy cell: when a switch turns ON, energy is stored in the magnetizing inductance, and during the OFF interval it is delivered through the secondary and diode to the weaker cell [14], [17].

International Journal of Engineering Research & Technology (IJERT)
ISSN: 2278-0181
Vol. 15 Issue 06 , June - 2026

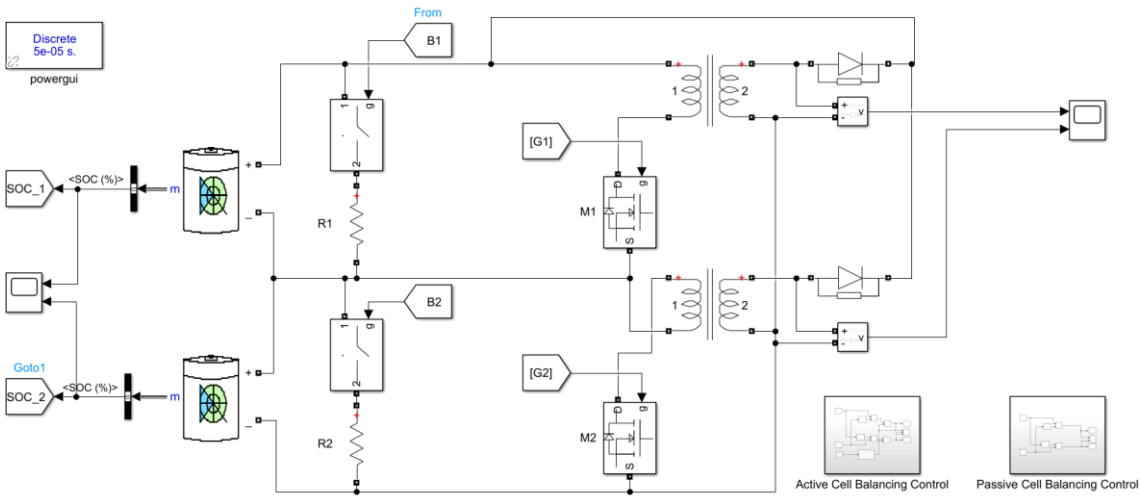

Fig. 3. MATLAB/Simulink model of passive and active cell balancing with the flyback converter.

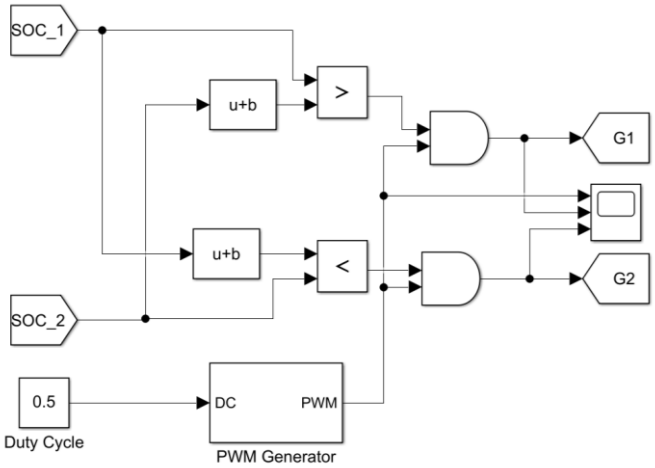

Fig. 4. Control logic generating the gate pulses for active cell balancing.

The system specifications used in the simulation are listed in Table I. Two initial-SOC scenarios are considered: Case a, in which Cell 1 starts higher than Cell 2, and Case b, in which Cell 2 starts higher than Cell 1. Performance is measured in terms of accurate SOC equalization in discharge mode and the time taken to balance.

TABLE I. System Specification for Simulation

Particulars	Value
Cell 1	3.7 V, 5.4 Ah
Cell 2	3.7 V, 5.4 Ah
DC–DC converter	Flyback converter
Transformer ratio	1:3
Control strategy	SOC-based balancing algorithm
Case a: initial SOC	Cell 1: 80%, Cell 2: 75%
Case b: initial SOC	Cell 1: 70%, Cell 2: 75%
Passive balancing resistor	2 Ω

B. Passive Balancing Results

International Journal of Engineering Research & Technology (IJERT)
ISSN: 2278-0181
Vol. 15 Issue 06 , June - 2026

The passive model was executed for 500 s. In Case a (Cell 1 = 80%, Cell 2 = 75%) the algorithm closes the Cell-1 switch, forcing Cell 1 to discharge through its balancing resistor until its SOC drops to that of Cell 2. The SOC trajectories are shown in Fig. 5. Switch S1 remains ON and S2 OFF until balancing completes in 484 s, after which both switches open and the pack settles at 75%. In Case b (Cell 1 = 70%, Cell 2 = 75%) the Cell-2 switch is closed instead, and the cells equalize at 70% in the same 484 s. In both cases the pack balances down to the SOC of the weakest cell, confirming the energy-wasting nature of passive balancing.

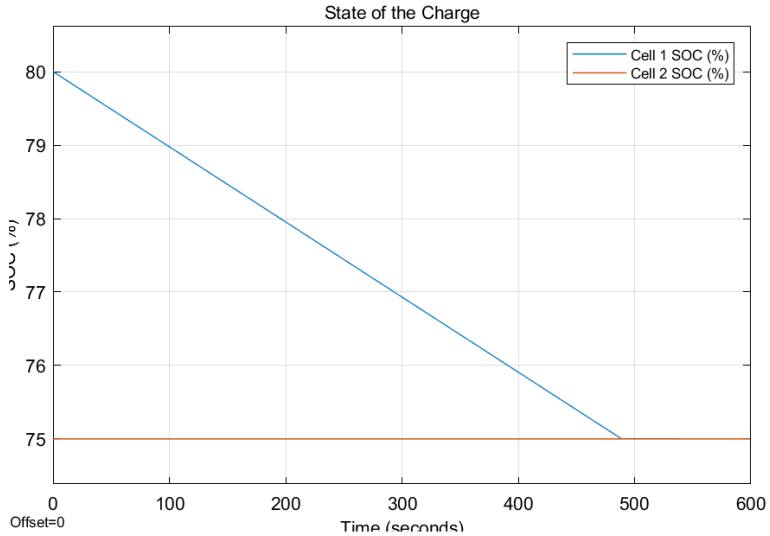

Fig. 5. SOC of Cell 1 and Cell 2 during passive balancing (Case a).

C. Active Balancing Results

The active flyback model was executed for 350 s. In Case a, where Cell 1 has the higher SOC, the algorithm applies PWM pulses to MOSFET M1 while M2 stays OFF. Energy drains from Cell 1 through the transformer, is rectified at the secondary, and is returned to the pack so that Cell 2 charges up. The SOC trajectories of Fig. 6 show that the 5% mismatch is eliminated in 235 s, with the corresponding triggering pulses shown in Fig. 7.

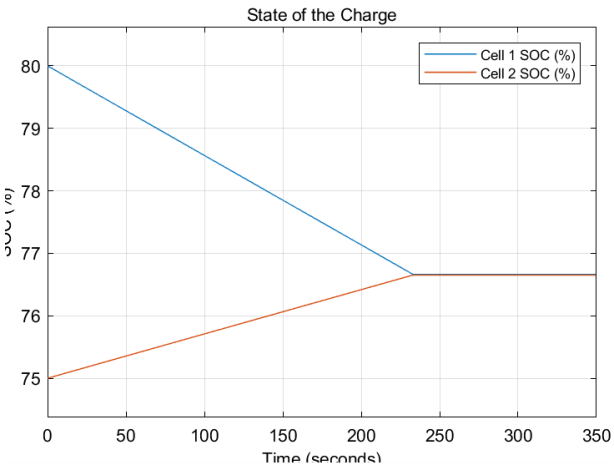

Fig. 6. SOC of Cell 1 and Cell 2 during active balancing (Case a).

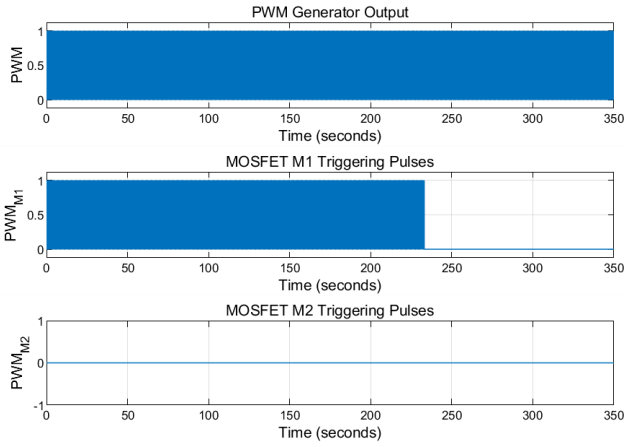

Fig. 7. PWM triggering pulses during active balancing (Case a).

In Case b the situation is reversed: Cell 2 is the source, so M2 is pulsed and M1 stays OFF, transferring energy to Cell 1. As shown in Fig. 8 and Fig. 9, the 5% mismatch is again balanced in 235 s, identical to Case a, demonstrating the symmetry of the bidirectional energy-routing scheme.

International Journal of Engineering Research & Technology (IJERT)
ISSN: 2278-0181
Vol. 15 Issue 06 , June - 2026

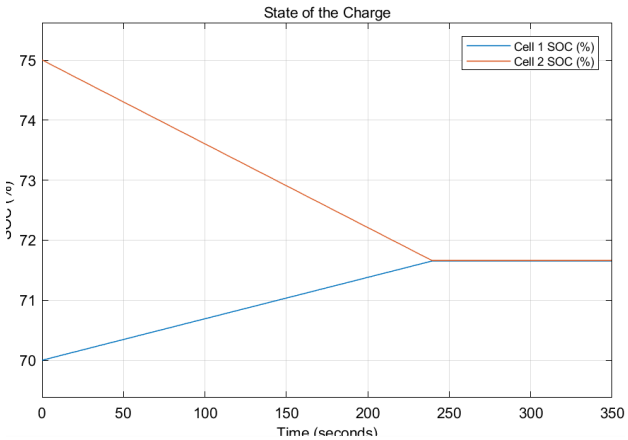

Fig. 8. SOC of Cell 1 and Cell 2 during active balancing (Case b).

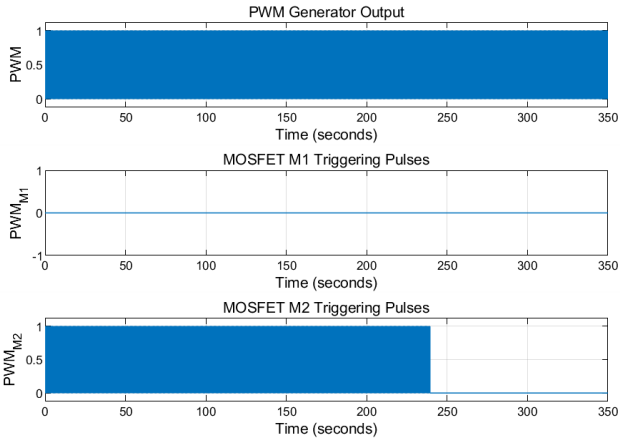

Fig. 9. PWM triggering pulses during active balancing (Case b).

From these results the balancing time depends on the initial SOC difference; for the active flyback scheme the balancing speed is 47s per percent of SOC, against roughly 96 s per percent for the passive resistive scheme. The active method therefore balances about twice as fast while conserving rather than dissipating the transferred energy, in agreement with reported flyback-based designs [16], [17], [20].

IV. HARDWARE IMPLEMENTATION AND EXPERIMENTAL RESULTS

A. Proposed System and Component Selection

To validate the simulation, a hardware prototype combining passive and active balancing with a flyback converter was built for the specifications of Table II. The block diagram comprises the battery pack, a voltage-sensing and SOC-estimation unit, an Arduino-based controller, a passive/active mode-selection stage, the flyback converter, a relay circuit for the resistive path and an LCD display. The controller compares the two cell voltages against threshold limits and selects passive balancing for small imbalances or active flyback balancing for larger ones, generating the relay and MOSFET switching signals accordingly.

TABLE II. Specifications of the Hardware Prototype

Particulars	Value
Cell 1	3.7 V, 2.4 Ah
Cell 2	3.7 V, 2.4 Ah
DC–DC converter	Flyback converter
Transformer ratio	1:3
Control strategy	SOC-based balancing algorithm
Passive balancing resistor	10 Ω, 5 W

Two series-connected 3.7 V, 2400 mAh lithium-ion cells form the pack. Each cell voltage is scaled to the Arduino 5 V range by a resistive voltage divider, $V_{out} = R_2 / (R_1 + R_2) \cdot V_{in}$. With R_2 = 1 kΩ and a 50 V maximum input, R_1 works out to about 9 kΩ, so standard values of R_1 = 10 kΩ and R_2 = 1 kΩ (0.25 W) are used.

A custom high-frequency transformer (1 A, 1:3 turns ratio, 20 kHz) is used as the coupled inductor. For a 3.7 V input, 10 V target output and 5 W transfer the load current is about 0.5 A; allowing twice the working current and three times the working voltage as a safe-operating-area margin, an IRFZ44 MOSFET (V_{DSS} = 60 V, I_D = 15 A) is selected for switching and a 1N4007 diode (1000 V PIV, 1 A) for rectification. A PC817 optocoupler isolates and drives each gate, while an Arduino Uno (ATmega328, six ADC inputs, six PWM outputs, 14 digital I/O) performs voltage measurement, SOC estimation, relay control and PWM generation. A 16×2 LCD displays the cell voltages and balancing status.

International Journal of Engineering Research & Technology (IJERT)
ISSN: 2278-0181
Vol. 15 Issue 06 , June - 2026

B. Circuit Diagram and Programming

The complete circuit, Fig. 10, balances Cell 1 and Cell 2 by transferring energy through the isolated flyback transformers TR1 and TR2 during active balancing or by dissipating it in a discharge resistor during passive balancing. The Arduino reads both cell voltages on its analog pins, decides which cell needs balancing, and drives the appropriate relay and MOSFET. During the MOSFET ON time, energy is stored in the transformer magnetic field; during the OFF time, the stored energy is delivered through the secondary winding and rectifier diode to the lower-voltage cell. The PC817 optocouplers protect the controller from switching transients, and the secondary diodes D1 and D2 enforce unidirectional energy flow.

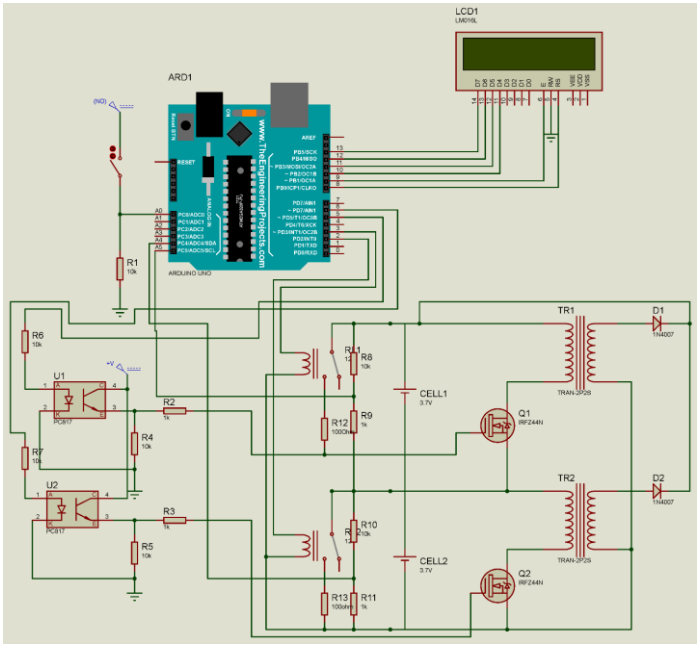

Fig. 10. Circuit diagram of the passive and active cell-balancing system using flyback converters.

The firmware follows the SOC-based balancing logic of Section II-C. In active mode the controller measures the SOC of both cells, compares them, and starts the converter associated with the higher-SOC cell so that energy is transferred to the lower-SOC cell, repeating until the SOC values are equal. In passive mode the controller compares the SOC values and energizes the relay of the higher-SOC cell, dissipating its excess charge through the resistive path until equality is reached.

C. Experimental Results

The prototype, shown in Fig. 11, was operated in both balancing modes. In passive mode the discharge resistor is switched across the cell holding the higher SOC, discharging it down to the level of the other cell, as recorded in Table III.

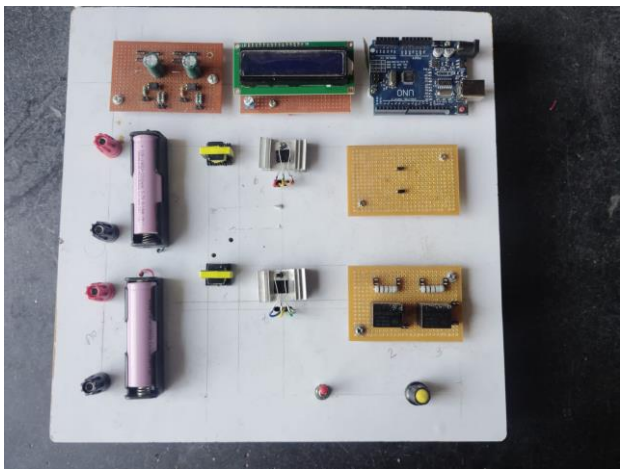

Fig. 11. Experimental setup of the developed passive and active cell-balancing prototype.

TABLE III. Observations of Passive Cell Balancing

International Journal of Engineering Research & Technology (IJERT)
ISSN: 2278-0181
Vol. 15 Issue 06 , June - 2026

Initial SOC	Relay 1	Relay 2	Final SOC	Time (s)
Cell 1: 85%, Cell 2: 70%	ON	OFF	Cell 1: 70%, Cell 2: 70%	1420
Cell 1: 75%, Cell 2: 85%	OFF	ON	Cell 1: 75%, Cell 2: 75%	950
Cell 1: 70%, Cell 2: 70%	OFF	OFF	Cell 1: 70%, Cell 2: 70%	—

Passive balancing of a 10% imbalance took 950 s, i.e. about 95 s per percent of SOC, and again equalized the pack at the lower cell level. In active mode the controller estimates the SOC of each cell and triggers the appropriate flyback converter to transfer energy to the weaker cell; the observations are given in Table IV.

TABLE IV. Observations of Active Cell Balancing

Initial SOC	Conv. 1	Conv. 2	Final SOC	Time (s)
Cell 1: 85%, Cell 2: 70%	Active	OFF	Cell 1: 70%, Cell 2: 70%	1140
Cell 1: 75%, Cell 2: 85%	OFF	Active	Cell 1: 75%, Cell 2: 75%	760
Cell 1: 70%, Cell 2: 70%	OFF	OFF	Cell 1: 70%, Cell 2: 70%	—

Active balancing of the same 10% imbalance took 760 s, i.e. about 76 s per percent of SOC — roughly 20% faster than the passive prototype and without the resistive energy loss. The slightly higher per-percent time compared with the 47 s/percent obtained in simulation is attributed to practical delays in SOC estimation and to component tolerances and mismatch in the hardware. The measured gate-pulse and flyback output-voltage waveforms confirmed correct PWM switching and energy transfer during operation.

D. Discussion

Table V consolidates the balancing-speed metrics. In both simulation and hardware the active flyback scheme outperforms the passive resistive scheme, and the key qualitative advantage is that active balancing redistributes energy within the pack rather than wasting it as heat. This conserves usable capacity, reduces localized thermal stress and is therefore better suited to high-energy EV and stationary-storage packs [10], [11], [18]. The galvanic isolation provided by the flyback transformer additionally improves safety and scalability to higher-voltage strings [14], [16].

TABLE V. Comparison of Balancing Speed

Method / Platform	Imbalance	Total time	Per % SOC
Passive – Simulation	5%	484 s	≈ 96 s
Active – Simulation	5%	235 s	47 s
Passive – Hardware	10%	950 s	95 s
Active – Hardware	10%	760 s	76 s

V. CONCLUSION AND FUTURE SCOPE

This work designed, simulated and experimentally implemented passive and active cell balancing for two series-connected lithium-ion cells, using an isolated flyback converter for cell-to-pack energy transfer in the active mode and resistive dissipation in the passive mode. A SOC-based algorithm controlled the converter duty cycle and gate pulses. In simulation the passive scheme balanced a 5% imbalance in about 96 s per percent, while the active flyback scheme achieved 47 s per percent. The hardware prototype balanced a 10% imbalance in 95 s per percent passively and 76 s per percent actively, the modest gap from the simulated active figure being due to SOC-estimation delays and component tolerances. Across both platforms the flyback-based active method balanced faster and, more importantly, conserved energy rather than dissipating it, while its galvanic isolation enhanced safety and scalability. These results confirm that flyback-converter active balancing is an effective and practical solution for lithium-ion battery management in electric vehicles and energy-storage systems [16]–[18].

International Journal of Engineering Research & Technology (IJERT)
ISSN: 2278-0181
Vol. 15 Issue 06 , June - 2026

Future work will focus on optimizing the transformer magnetics and applying soft-switching techniques such as zero-voltage and zero-current switching to reduce switching and core losses and shrink the converter footprint [15]. Extending the scheme to multi-cell, high-voltage strings, augmenting voltage-based balancing with SOC and state-of-health estimation, and integrating machine-learning-based predictive control are promising directions for next-generation, intelligent and modular battery management systems [6], [21].

REFERENCES

[1] A. Manthiram, "An outlook on lithium-ion battery technology," ACS Central Science, vol. 3, no. 9, pp. 1063–1069, 2017.
[2] X. Wang, S. Li, L. Wang, Y. Sun and Z. Wang, "Degradation and dependence analysis of a lithium-ion battery pack in the unbalanced state," Energies, vol. 13, no. 22, p. 5934, 2020.
[3] M. Naylor Marlow, J. Chen and B. Wu, "Degradation in parallel-connected lithium-ion battery packs under thermal gradients," Communications Engineering, vol. 3, no. 1, 2024.
[4] R. D. Anderson, R. Zane, G. Plett, D. Maksimovic, K. Smith and M. S. Trimboli, "Life balancing – a better way to balance large batteries," SAE Technical Paper 2017-01-1210, 2017.
[5] J. Joshi and J. Thakkar, "Active cell equalization for battery management systems: a comprehensive review of DC–DC converter topologies," Energy Engineering, vol. 123, no. 4, pp. 1–25, 2026.
[6] Safari, H. Sorouri, A. Oshnoei et al., "A state-of-the-art review on battery cell balancing strategies," Discover Energy, vol. 5, no. 31, 2025.
[7] R. Ahmed, M. S. Khalid and A. Abbas, "Adaptive recombination-based control strategy for cell balancing in lithium-ion battery packs: modeling and simulation," Electronics, vol. 14, no. 11, p. 2217, 2025.
[8] H. Wang, J. Zhang and L. Zhao, "Li-ion battery active–passive hybrid equalization topology for low-earth orbit power systems," Energies, vol. 18, no. 10, p. 2463, 2025.
[9] K. L. S. Mohitha, N. K. Tadikonda, T. Kiran, P. Sravani and K. Nikhil, "Efficient battery management using cell balancing techniques," in Proc. 2024 Int. BIT Conf. (BITCON), Dhanbad, India, 2024, pp. 1–6.
[10] N. Ghaeminezhad, Q. Ouyang, X. Hu, G. Xu and Z. Wang, "Active cell equalization topologies analysis for battery packs: a systematic review," IEEE Trans. Power Electron., vol. 36, no. 8, pp. 9119–9135, 2021.
[11] Z. B. Omariba, L. Zhang and D. Sun, "Review of battery cell balancing methodologies for optimizing battery pack performance in electric vehicles," IEEE Access, vol. 7, pp. 129335–129352, 2019.
[12] P. Jadhav, M. Murali, A. Bagade and A. Mandhana, "Comparative analysis of cell balancing techniques and development of an active cell balancing model using an inductor," in Proc. 2023 5th Int. Conf. Energy, Power and Environment (ICEPE), Shillong, India, 2023, pp. 1–6.
[13] K. H. Patel, P. B. Darji and J. G. T. Viswanathan, "Analysis of active cell balancing topologies with electrical cell modeling techniques," in Proc. 2023 11th Nat. Power Electron. Conf. (NPEC), Guwahati, India, 2023, pp. 1–6.
[14] P. D. Inamati, K. B. Meti, R. D. Gaddanakeri, H. R. Patil, A. Patil and A. B. Raju, "Active cell balancing using isolated converters," in Proc. 2022 Int. Conf. Smart Generation Computing, Communication and Networking (SMART GENCON), Bangalore, India, 2022, pp. 1–6.
[15] F. Forest, E. Laboure, T. A. Meynard and J.-J. Huselstein, "Multicell interleaved flyback using intercell transformers," IEEE Trans. Power Electron., vol. 22, no. 5, pp. 1662–1671, 2007.
[16] L. Otunubi, E. A. Thompson, J. Bender and J. Eitsert, "Active LiFePO4 battery cell balancing based on a flyback converter for battery storage application," in Proc. 2024 IEEE 12th Int. Conf. Smart Energy Grid Eng. (SEGE), Oshawa, Canada, 2024, pp. 241–244.
[17] A. Brandis, D. Pelin, D. Topić and B. Tomašević, "Active Li-ion battery charge balancing system based on a flyback converter," in Proc. 2020 IEEE 11th Int. Symp. Power Electron. Distrib. Gen. Syst. (PEDG), Dubrovnik, Croatia, 2020, pp. 164–169.
[18] X. Guo, J. Geng, Z. Liu, X. Xu and W. Cao, "A flyback converter-based hybrid balancing method for series-connected battery packs in electric vehicles," IEEE Trans. Veh. Technol., vol. 70, no. 7, pp. 6626–6635, 2021.
[19] M. Raeber, A. Heinzelmann and D. O. Abdeslam, "Analysis of an active charge balancing method based on a single non-isolated DC/DC converter," IEEE Trans. Ind. Electron., vol. 68, no. 3, pp. 2257–2265, 2021.
[20] L. Tian, M. Hong, Z. He and M. Gao, "Active battery balancing circuit based on an optimized flyback converter for large lithium-ion battery packs," in Proc. 2018 IEEE 4th Int. Conf. Control Science and Systems Eng. (ICCSSE), Wuhan, China, 2018, pp. 212–216.
[21] A. Ziegler, D. Oeser, T. Hein, D. Montesinos-Miracle and A. Ackva, "Reducing cell-to-cell variation of lithium-ion battery packs during operation," IEEE Access, vol. 9, pp. 24994–25001, 2021.
[22] R. Paidi and S. K. Gudey, "Active and passive cell balancing techniques for Li-ion batteries used in EVs," in Proc. 2022 IEEE Int. Power and Renewable Energy Conf. (IPRECON), Kollam, India, 2022, pp. 1–6.
[23] M. Daowd, N. Omar, P. Van Den Bossche and J. Van Mierlo, "Passive and active battery balancing comparison based on MATLAB simulation," in Proc. 2011 IEEE Vehicle Power and Propulsion Conf. (VPPC), 2011, pp. 1–7.
[24] J. F. Reynaud, C. E. Carrejo, O. Gantet, P. Aloïsi, B. Estibals and C. Alonso, "Active balancing circuit for advanced lithium-ion batteries used in photovoltaic applications," Renew. Energy Power Qual. J., vol. 9, 2011.
[25] P. Bhanu, K. Deekshitha, V. Jayanth and V. Sandeep, "Comparative performance analysis of buck-boost, SEPIC and Zeta converters for active cell balancing in EV batteries," in Proc. 2024 Int. Conf. Social and Sustainable Innovations in Technology and Eng. (SASI-ITE), 2024, pp. 224–229.
[26] NXP Semiconductors, "Active cell balancing in battery packs," Application Note AN4428, Rev. 0, 2012.
[27] C.-D. Téllez-Uribe et al., "Comparison of balancing methods for LiPo cells energy storage at medium power ratings," in Proc. 2024 IEEE Int. Autumn Meeting on Power, Electronics and Computing (ROPEC), 2024, pp. 1–7.
[28] C. Wang, F. Li, Y. Cao, M. Dong and M. Li, "Active SOC balancing structure using parallel low-power DC-DC converters for electric vehicles," in Proc. 2022 41st Chinese Control Conf. (CCC), 2022, pp. 5165–5169.